Journal of Experimental Botany, Vol. 76, No. 12 pp. 3345–3358, 2025
https://doi.org/10.1093/jxb/eraf151 Advance Access Publication 10 April 2025

RESEARCH PAPER

GIBBERELLIN 3-OXIDASE genes regulate height and grain size in bread wheat

Andrew L. Phillips[1], Alison K. Huttly[1], Rocío Alarcón-Reverte[1], Suzanne J. Clark[1], Pavel Jaworek[2], Danuše Tarkowská[2], Patrycja Sokolowska[1], David Steele[1], Andrew Riche[1], Malcolm J. Hawkesford[1], Stephen G. Thomas[1], Peter Hedden[1,2], and Stephen Pearce[1,*]

[1] Rothamsted Research, Harpenden, Hertfordshire AL5 2JQ, UK
[2] Laboratory of Growth Regulators, Institute of Experimental Botany, Czech Academy of Sciences and Palacký University Olomouc, Šlechtitelů 27, CZ-77900 Olomouc, Czech Republic

* Correspondence: stephen.pearce@rothamsted.ac.uk

Received 27 January 2025; Editorial decision 1 April 2025; Accepted 3 April 2025

Editor: Mary Byrne, University of Sydney, Australia

Abstract

Plant gibberellin (GA) concentrations are tightly regulated to optimize growth and development. GA 3-oxidases (GA3OX) catalyse a key GA biosynthesis step, converting precursor GAs into bioactive forms. We characterized seven *GA3OX* homologues in bread wheat (*Triticum aestivum* L.): a homoeologous triad of *GA3OX2* genes expressed in vegetative and reproductive tissues, and four others (a homoeologous triad of *GA3OX3* genes plus *GA1OX1-B1*) expressed predominantly in grains. *ga3ox2* mutants are severely dwarfed and infertile due to very low bioactive GA concentrations, indicating that *GA3OX2* is essential for normal wheat development. By contrast, *ga3ox3* mutants have lower bioactive GA concentrations in grains, reducing grain size and weight, whereas *ga1ox1* mutants accumulate high concentrations of bioactive GAs, producing larger grains. Unexpectedly, *ga3ox3* and *ga1ox1* alleles also affected height, possibly reflecting GA transport to vegetative tissues. Natural variation in adjacent *GA3OX3-B1* and *GA1OX1-B1* genes was associated with differences in grain size and weight, suggesting that a haplotype associated with larger grains was selected during modern breeding. Our study shows that the wheat *GA3OX* family has diversified roles, with *GA3OX2* required for general growth and *GA3OX3*/*GA1OX1* modulating GA concentrations during grain development. These findings highlight opportunities to exploit variation in GA biosynthetic pathways for wheat improvement.

Keywords: GA 3-oxidase, genetic diversity, gibberellin, grain size, height, wheat.

Introduction

Gibberellins (GAs) are a family of diterpenoid carboxylic acids, members of which function as hormone signals in higher plants, regulating important developmental processes such as seed germination, stem elongation, and flowering (Castro-Camba *et al.*, 2022). Of the 136 identified GA forms, only a few, primarily GA_1, GA_4 and GA_3, exhibit bioactivity (Sponsel, 2016). These bioactive GAs bind to the receptor GIBBERELLIN INSENSITIVE DWARF1 (GID1), triggering a conformational change that enhances the affinity of GID1 for DELLA proteins, resulting in the latter protein's

Abbreviations: 2-ODD, 2-oxoglutarate-dependent dioxygenase; GA, gibberellin; GA20OX, GA 20-oxidase; GA2OX, GA 2-oxidase; GA3OX, GA 3-oxidase; EMS, ethyl methanesulfonate; LMM, linear mixed model; REML, restricted maximum likelihood; TGW, thousand-grain weight.

polyubiquitination and degradation via the E3-ubiquitin ligase pathway (Ueguchi-Tanaka *et al.*, 2005; de Lucas *et al.*, 2008; Shimada *et al.*, 2008). DELLA proteins modulate the activity of hundreds of transcription factors through protein–protein interactions, and their GA-mediated degradation has a major effect on the cellular transcriptional landscape (Zentella *et al.*, 2007). Therefore, it is essential that the concentrations of bioactive GAs are tightly controlled to ensure optimal growth responses to developmental signals and environmental cues (Shani *et al.*, 2024).

Plants precisely regulate their bioactive GA concentrations through the activity of different classes of GA biosynthetic enzymes (Shani *et al.*, 2024). Four classes of 2-oxoglutarate-dependent dioxygenases (2-ODDs), GA 20-oxidase (GA20OX), GA 3-oxidase (GA3OX), C_{19}-GA 2-oxidase (C_{19}GA2OX), and C_{20}-GA 2-oxidase (C_{20}GA2OX), catalyse key steps in the final stages of GA biosynthesis (GA20OX and GA3OX) and inactivation (C_{19}GA2OX and C_{20}GA2OX) (Fig. 1). Each enzyme contains a conserved core domain that binds ferrous Fe (Fe^{2+}) as a cofactor, which is required to catalyse the oxidation of GA substrates in the presence of the co-substrates O_2 and 2-oxoglutarate (Kawai *et al.*, 2014). Their activity is a major factor in determining the concentration of bioactive GAs.

The GA biosynthetic pathway splits into the non-13-hydroxylation (13-H) or 13-hydroxylation (13-OH) branches depending on the 13-hydroxylation of GA_{12}, which is catalysed by the cytochrome P450 GA 13-oxidase (Fig. 1). In each branch, GA20OX enzymes catalyse three consecutive oxidation reactions on C-20, producing GA_9 and GA_{20} from GA_{12} and GA_{53}, respectively (Fig. 1). These GAs are substrates for GA3OX enzymes, which catalyse the 3β-hydroxylation of GA_9 to bioactive GA_4 and GA_{20} to bioactive GA_1 (Appleford *et al.*

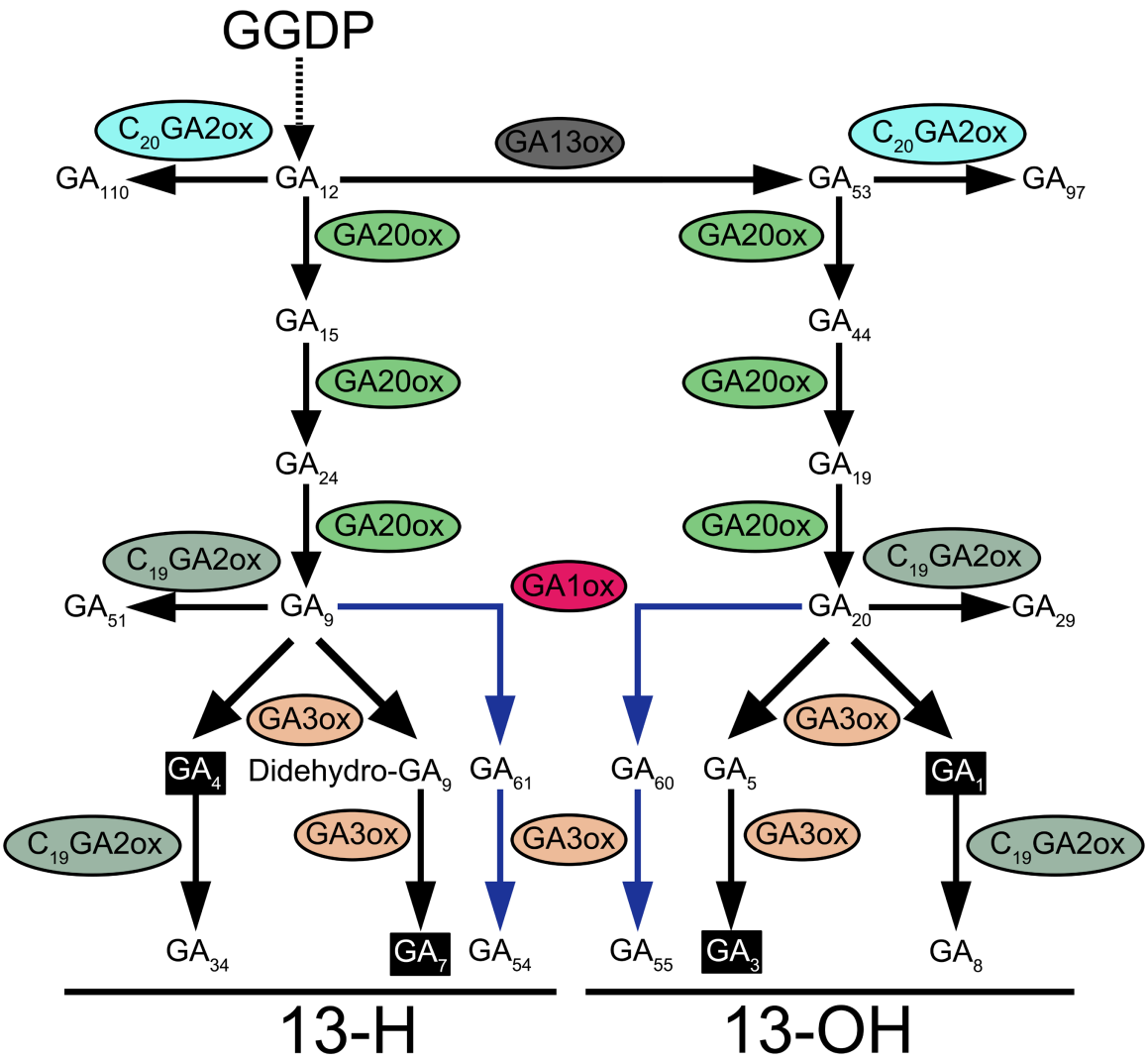

Fig. 1. Late stages of the gibberellin (GA) biosynthesis pathway in higher plants showing the activity and substrates of 2-ODD enzymes. Substrates GA_{54}, GA_{55}, GA_{60} and GA_{61} are detected only in wheat grain tissues. The reactions forming these substrates are highlighted in blue.

2006) (Fig. 1). The two classes of GA2OX enzymes catalyse the 2β-hydroxylation of bioactive (C_{19}) or precursor (C_{20}) GAs, respectively, at the C-2 position, resulting in their inactivation, thus reducing the pool of bioactive GAs (Thomas *et al.*, 1999; Schomburg *et al.*, 2003). GA-mediated degradation of DELLA proteins suppresses *GA20OX* and *GA3OX* expression and promotes *GA2OX* expression as a homeostatic mechanism controlling the rate of GA biosynthesis (Zentella *et al.*, 2007).

GA20OX, GA3OX, and GA2OX enzymes are encoded by multigene families in the genomes of all seed plants (Kawai *et al.*, 2014). These gene families have undergone lineage-specific expansions and functional diversification. The Arabidopsis genome contains four *GA3OX* genes, including *AtGA3OX1* and *AtGA3OX2*, which redundantly regulate vegetative development (Mitchum *et al.*, 2006). However, paralogous *GA3OX* genes in Arabidopsis and *Oryza* species are grouped into different phylogenetic subclades, indicating that these families have expanded independently since the monocot–dicot divergence (Kawai *et al.*, 2014; Pearce *et al.*, 2015; Wang *et al.*, 2023). Monocot genomes contain at least two paralogues of *GA3OX*, including highly conserved *GA3OX2* genes that play a critical role in vegetative development. In rice (*Oryza sativa*), a null allele of *OsGA3OX2* (*d18-AD*) confers a severely dwarfed growth habit, stunted stems, and wide, dark-green leaves (Itoh *et al.*, 2001; Sakamoto *et al.*, 2004). The *GA3OX* family also underwent independent expansion and functional divergence in different monocot tribes. In rice, *OsGA3OX1* is expressed in anther filaments, lodicules, and pollen, and is required for male reproductive development (Kawai *et al.*, 2022; Hsieh *et al.*, 2023). Transcripts are also detected in the epithelium of the embryo scutellum, suggesting a role in germination (Kaneko *et al.*, 2003). However, in other *Oryza* species, such as *Oryza punctata*, the orthologous gene is expressed in roots and spikelet tissues as well as anthers, suggesting that the specialized role of *OsGA3OX1* in reproductive development has evolved recently in *O. sativa* (Kawai *et al.*, 2022).

Barley (*Hordeum vulgare*) and wheat (*Triticum* species) genomes do not contain orthologues of *OsGA3OX1*. An independent duplication event in the Triticeae originated the orthologues *HvGA3,18OX1* in barley and *GA3OX3* in wheat (Pearce *et al.*, 2015). Both genes are highly expressed in grain tissues but encode enzymes with distinct biochemical activity. In barley, *HvGA3,18OX1* encodes a bifunctional GA 3β,18-dihydroxylase enzyme that catalyses the conversion of GA_9 to GA_{131}, whereas in wheat, *GA3OX3* catalyses the 3β-hydroxylation of GA_9 to bioactive GA_4 and of GA_{61} to GA_{54} (Fig. 1). A tandem duplication on chromosome 2B specific to wheat originated *GA1OX1-B1*, which encodes a GA 1-oxidase that catalyses the conversion of GA_9 to GA_{61} (Pearce *et al.*, 2015; Wang *et al.*, 2023). In addition to GA_{61} and GA_{54}, developing wheat grains contain their 13-OH analogues GA_{60} and GA_{55}, respectively (Gaskin *et al.*, 1980; Kirkwood and MacMillan, 1982). Based on their biochemical activity, we proposed that TaGA1OX1-B1 and TaGA3OX3 act sequentially to catalyse GA_{54}/GA_{55} synthesis from GA_9/GA_{20}, respectively, during grain development, although the physiological relevance of this activity remains unknown (Pearce *et al.*, 2015).

The goal of the current study was to determine the function of *GA3OX2*, *GA3OX3*, and *GA1OX1* in wheat. Using stacked ethyl methanesulfonate (EMS)-induced loss-of-function mutant lines, we showed that *GA3OX2* activity is essential for normal vegetative and reproductive development. *ga3ox3* mutants exhibited reduced bioactive GA concentrations, grain weight, and height, whereas *ga1ox1* mutants accumulated high concentrations of bioactive GA and had larger grains and increased height. Natural genetic variation at the *GA3OX3-B1-GA1OX1-B1* locus was associated with grain size in a collection of wheat landraces. Our research provides insight into the functional divergence of GA biosynthesis enzymes in wheat and highlights the potential to exploit variation in GA biosynthetic pathways for crop improvement.

Materials and methods

Plant materials and growth conditions

Wheat (*Triticum aestivum* L.) lines carrying mutations in the target *GA3OX* and *GA1OX* genes were identified from an *in silico* database of wheat EMS mutants in the 'Cadenza' genetic background (Krasileva *et al.*, 2017) (Table 1). Individual M_4 lines carrying mutations in different homoeologous copies of each target gene were combined by crossing, backcrossed to wild-type 'Cadenza' to reduce the number of background mutations, and then selfed to select wild-type and mutant sister lines for each target gene. All selected mutations introduce premature stop codons upstream of essential protein domains except the *ga1ox1* mutant, which carries a point mutation in the 3′ splice acceptor site of intron 2 (Supplementary Fig. S1). With such mutations, there is a risk that the presence of alternate in-frame splice sites can result in the translation of a functional allele. However, the extremely low concentrations of GA_{54} and GA_{61} in these mutant lines suggest that the *ga1ox1* allele encodes a non-functional protein.

Seeds were germinated on damp filter paper, transferred to 2 cm × 2 cm cells of Rothamsted Prescription Mix compost, then moved to 15 cm pots and grown under standard glasshouse conditions. Glasshouse phenotyping of *ga3ox2* genotypes was performed using BC_3F_2 plants.

Table 1. EMS-induced mutations in *GA3OX2*, *GA3OX3,* and *GA1OX1* used in this study

Target gene	IWGSC v2.1 gene ID	Line number	Functional effect on the protein
GA3OX2-A1	*TraesCS3A03G0268400*	Cadenza1176	W149*
GA3OX2-B1	*TraesCS3B03G0336700*	Cadenza0110	W130*
GA3OX2-D1	*TraesCS3D03G0261200*	Cadenza0268	W149*
GA3OX3-A1	*TraesCS2A03G1246800*	Cadenza0593	W71*
GA3OX3-B1	*TraesCS2B03G1429200*	Cadenza1640	R172*
GA3OX3-D1	*TraesCS2D03G1203500*	–	–
GA1OX1-B1	*TraesCS2B03G1429000*	Cadenza1684	3′ splice acceptor intron 2

In 'Cadenza', *GA3OX3-D1* encodes a non-functional protein due to a 7 bp insertion in exon 2 that disrupts the open reading frame.

Twice-weekly foliar sprays of 10 μM GA_3 were required to initiate flowering and seed setting. Glasshouse phenotyping of *ga3ox3* genotypes was performed using BC_3F_3 plants, and field experiments used BC_3F_4 and BC_3F_5 lines. Glasshouse phenotyping of *ga1ox1* genotypes was performed using BC_5F_3 plants, and field experiments used BC_5F_4 and BC_5F_5 lines.

Glasshouse experiments

Plant height was determined in the glasshouse using a randomized extended block design consisting of four blocks of 18 pots with three plants per pot. The trial included 10 lines in total but only the results for *ga3ox3*, *ga1ox1*, and their corresponding wild-type controls are presented here. Each genotype was grown in two pots per block so that a total of 24 plants in eight pots were phenotyped for each line. Mean heights were compared using one-way ANOVA with a nested blocking structure (block/pot/plant), incorporating nested mutant versus wild-type contrasts for each gene. Heights were $\log_{10}$ transformed before analysis to achieve variance homogeneity. Tiller number and spikelet number were measured for *ga3ox2* in a separate glasshouse trial grown as a single block and compared using Student's *t*-test (n=20). Inflorescence development in these lines was assessed using manual dissection and imaging on a Leica M205 FA stereomicroscope with DFC310 FX camera and Leica LAS X software (Leica Microsystems, Milton Keynes, UK).

Field experiments

Field experiments were sown in spring 2021 and autumn 2023 at Rothamsted Research Experimental Farm in southeast England as 1 m^2 plots with a seeding rate of 450 seeds m^{-2} using standard farm practice for fertilizer and pesticide application. No plant growth regulators were applied. The 2021 field trial plan comprised three replicate blocks arranged as arrays of six rows and six columns, with the complete trial arranged as 18 rows by six columns. Lines were allocated to plots in each trial according to a resolvable row–column design with blocking as described and additional Latinization across 'long columns' (i.e. single columns of 18 plots cutting across the replicate blocks) to allow for potential additional variation due to the direction of farming operations (perpendicular to spatial blocking). The 2023 field experiment had the same overall 18 × 6 layout as in the 2021 experiment but comprised six three-row by six-column replicate blocks, with long columns of 18 plots again cutting across blocks. Each trial included multiple lines but only the results for *ga3ox3*, *ga1ox1*, and their corresponding wild-type controls are presented here. An error during drilling of the 2023 trial meant that the blocks no longer contained a complete replicate of the 18 genotypes tested. However, the analysis was still able to account for the design structure, enabling an appropriate comparison of the genotypes.

Height measurements in the field were taken using a floating polystyrene disc of diameter 60 cm, taking six measurements per plot. Samples for internode length, inflorescence, and grain measurements were taken from 10 randomly selected main tillers from each plot. Internode and spike lengths were measured manually between the lower bounds of each node. Grain sizes were measured on samples of ~200 grains using a MARVIN-Digital Seed Analyser (MARViTECH GmbH, Germany) running the software Marvin 6.0. Grain yield was measured at final harvest, as tonnes ha^{-1} corrected to 85% dry matter, calculated using the fresh weight of grain per plot and the grain dry matter content. Dry matter was calculated from the fresh and dry weight of a subsample of approximately 80 g dried for 16 h at 105 °C. Traits measured in both field trials were first analysed for each trial separately using linear mixed models (LMMs) fitted using restricted maximum likelihood (REML), each with a one-way fixed model (line) and the random model reflecting the design/randomization structure of the trial ((block/row)×long column in each case). Data from both trials were then combined using an LMM meta-analysis with a two-way (trial×line) fixed model and allowing a separate random model for each trial. Nested mutant versus wild-type contrasts were incorporated for each gene. The meta-analysis model allowed for separate estimates of the residual variance for each experiment, as well as for the different (but algebraically identical) random models.

Spikelet number, grain number, yield, and individual height components were measured only in 2023 and were analysed using an LMM fitted using REML, as described above. Nested mutant versus wild-type contrasts were incorporated for each gene.

The Watkins collection was sown at Rothamsted Farm in two consecutive years. The 2022 Watkins experiment was sown in autumn 2021 and harvested in summer 2022. The 2023 Watkins experiment was sown in autumn 2022 and harvested in summer 2023. Lines were allocated to one of six groups according to short/tall × early/middle/late characteristics. The six groups were allocated to main plots (20 × 6 arrays of field plots) within each of three blocks according to a randomized complete block design. Within main plots, lines (of a given group) were allocated to plots according to a resolvable row–column design. The 2023 trial was designed as a resolvable row–column design with three replicate blocks of 36 rows × 24 columns, 18-row Latinization, and overall size 36 rows × 72 columns. All plots were 1 m^2 sown at 300 seeds m^{-2}. A reduced rate of nitrogen fertilizer, 80 kg N ha^{-1}, was used to reduce the risk of lodging, and plant growth regulators were applied. Grain yield was calculated as described previously. Before harvest, 20 spikes were collected from a single plot for 618 lines in 2022 and for 810 lines in 2023, threshed using a laboratory thresher, and the grain and chaff samples were dried and weighed. From the data, the weight of grain per spike was calculated, and from the plot grain yield the number of spikes per unit area was calculated. A separate grain sample, saved from the combine harvester, was used for grain size measurements using a Marvin seed counter. The samples were then dried at 105 °C for 16 h, weighed, and the data were used to calculate the thousand-grain weight (TGW). From the TGW and grain yield, the number of grains per unit area was calculated, and then, using the spike population data, the number of grains per spike was calculated. Using the number of grains per spike and the chaff weight from threshing, the fruiting efficiency (grains per g of chaff) was calculated. All traits were measured in 2022; only spikes per m^2, grain weight per spike, and plot yield were measured in 2023. One-way ANOVA was used to determine the association between *GA3OX3-B1-GA1OX1-B1* haplotype and different phenotypic traits among the landraces. Fruiting efficiency values were $\log_{10}$ transformed to correct variance heterogeneity; all other traits are presented on the natural scale. Tukey's Honest Significant Difference post hoc test was used to determine significant differences between haplotype groups.

Haplotypes were compiled, analysed, and visualized using the package genHapR (Zhang *et al.*, 2023). Accession information, including genotype, ancestral group, and country of origin for the Watkins landraces, was previously described (Cheng *et al.*, 2024). Accessions with heterozygous base calls were excluded from the analysis. Contingency tables classified by haplotype and ancestral group or geographical region were analysed using Pearson's chi-squared test for association, with statistical significance calculated using a random permutation test as some expected values were small (<5).

Genotyping

Plants were genotyped using PCR Allele Competitive Extension (PACE) assays specific for each induced mutation. Haplotypes at the *GA3OX3-B1-GA1OX1-B1* locus were tested using two different PACE assays (Supplementary Table S1). Assays were run using an ABI7500 real-time PCR machine using 1× low-ROX PACE genotyping master mix (3CR Bioscience) using 250 ng of genomic DNA, 0.4 μM of the common primer, and 0.2 μM of each specific primer (Supplementary Table S1). The programme included 10 cycles of touchdown PCR (annealing

temperature ~63 °C, dropping by 0.5 °C per cycle) and 26 cycles of standard PCR (annealing temperature ~57 °C).

Quantification of gibberellins

Seven-day-old seedling tissues were harvested from BC_3F_2 *ga3ox2* mutant and wild-type 'Cadenza' plants, including the elongating leaf sheath region of the first leaf from the base to the lamina joint, including internal tissue such as developing leaves and the meristem. Five biological replicates of each genotype were harvested. To quantify the GA concentrations in grains, samples were harvested at 25 days post anthesis (DPA) from glasshouse-grown materials of BC_3F_2 lines of *ga3ox3* (wild-type, *ga3ox3-a1*, *ga3ox3-b1*, and *ga3ox3* genotypes) and BC_5F_2 lines of wild-type and *ga1ox1* genotypes. Freeze-dried samples (~5 mg) were processed, and GAs were quantified in five (seedling) or three/four (grain) biological replicates as described previously (Urbanová *et al.*, 2013). At the same stage of grain development, targeted analysis by combined GC-MS on a MAT95XP mass spectrometer coupled to a Trace GC (ThermoElectron) (MacMillan *et al.*, 1997) was used to detect the presence of GA_{54} in different wheat species.

Enzyme assays

Expression of *TaGA1ox1* in pET32b (Pearce *et al.*, 2015) in T7 chemically competent *Escherichia coli* (NEB) was induced in log phase with 0.5 mM IPTG followed by further cultivation at 20 °C for 16 h. Centrifuged cells were resuspended in 100 mM Tris–HCl buffer, pH 7.2, supplemented with 100 mM NaCl, 5% glycerol, and 2 mM DTT before disruption using a cell lyser (Constant Systems) at 186 MPa. The His-tagged TaGA1OX1 was purified on HisPur cobalt spin columns (Thermo Fisher Scientific), concentrated on Amicon centrifugal filters (Millipore) with a 30 kDa cutoff, and flash frozen in liquid nitrogen.

Assays to determine K_m and k_{cat} values for GA_9 and GA_{20} were performed as described previously (MacMillan *et al.*, 1997) with minor modifications. TaGA1ox1 was diluted to a final concentration of 100 nM and incubated with either substrate at 30 °C for 30 min in a 0.1–25 µM concentration range in a total volume of 55 µl. To stop the reaction, methanol and acetic acid were added to reach 33% and 3.3% of the total volume, respectively. The samples were analysed by LC-MS as described previously (Urbanová *et al.*, 2013) using single ion monitoring to determine the amounts of products formed. Parameters of Michaelis–Menten kinetics were calculated using GraphPad Prism 8.

The binding affinities of GA_9 and GA_{20} with TaGA1OX1 were determined by microscale thermophoresis on a Monolith NT.115 after labelling the enzyme with second-generation RED-tris-NTA dye (Nanotemper). A two-fold dilution series of both substrates was prepared, starting from 0.5 mM, and mixed with 50 nM labelled enzyme in 50 mM MOPS buffer at pH 7.5. The mixture also contained 4 mM DTT, 2.5% DMSO, 0.1% Tween-20, and 250 µM $FeSO_4$; 2-oxoglutarate and ascorbate were omitted to prevent enzymatic conversion.

Sequence analysis

We used BLASTn searches to identify *GA3OX2*, *GA3OX3*, and *GA1OX1* genes in the genome assemblies of sequenced wheat varieties and ancestors, including *Triticum urartu* accession G1812 (Ling *et al.*, 2018), *Aegilops longissima* accession AEG-6782-2, *Aegilops speltoides* ssp. *speltoides* accession AEG-9674-1 (Avni *et al.*, 2022), *Aegilops sharonensis* accession 1644 (line number BW_24933) (Yu *et al.*, 2022), *Aegilops tauschii* (accession AL8/78) (Luo *et al.*, 2017), *Triticum dicoccoides* 'Zavitan' (Avni *et al.*, 2017), and *Triticum durum* Svevo (Maccaferri *et al.*, 2019), as well as 13 varieties of *T. aestivum* (Walkowiak *et al.*, 2020) and *Triticum timopheevii* (Grewal *et al.*, 2024) (Supplementary Table S2). The microhomology tool in the online platform Triticeae Gene Tribe (Chen *et al.*, 2020) was used to present the physical location of *GA3OX* and *GA1OX1* genes.

Transcriptome analysis

Leaf sheath tissue from the grain to the top of the coleoptile was harvested from 7-day-old 'Cadenza' and *ga3ox2* mutant seedlings (four biological replicates each) and flash-frozen in liquid nitrogen. Total RNA was extracted using the Monarch® Total RNA Miniprep Kit with on-column DNase treatment (New England Biolabs, Ipswich, MA, USA). RNA quality was assessed using an Agilent RNA 6000 Nano Chip and Agilent 2100 Bioanalyzer (Agilent, Santa Clara, CA, USA). RNA samples were sequenced using paired-end Illumina sequencing by Novogene Europe (Cambridge, UK). Sequencing reads were trimmed for quality and adapter sequences using Trimmomatic 0.39 (parameters SLIDINGWINDOW:4:20; MINLEN:50) (Bolger *et al.*, 2014), then aligned and quantified using Kallisto against the IWGSC RefSeq v2.1 annotated gene models (Zhu *et al.*, 2021). Transcript per million values were calculated for each gene, and pairwise contrasts were made between 'Cadenza' and *ga3ox2* mutants using DESeq v2 (Love *et al.*, 2014).

Results

GA3OX2 is essential for wheat vegetative and reproductive development

Three wheat plants carrying EMS-induced mutations introducing premature stop codons in *GA3OX2-A1*, *GA3OX2-B1*, and *GA3OX2-D1*, respectively, were intercrossed, then backcrossed three times to wild-type 'Cadenza', to develop a *ga3ox2* mutant line (Table 1). All three mutant alleles encode truncated proteins that lack the essential Fe^{2+} 2-ODD catalytic domain and are highly likely to be non-functional (Supplementary Fig. S1A).

In seedling tissues, the concentration of bioactive GA_1 was approximately 3-fold lower in *ga3ox2* mutants than in wild-type 'Cadenza' ($P<0.001$), whereas GA_4 was not detected in any sample (Fig. 2A; Supplementary Table S3). The *ga3ox2* mutant accumulated significantly higher concentrations of GA_{20}, the substrate for GA3OX2, and GA_{29}, the 2β-hydroxylated inactivated product of GA_{20} (Fig. 2A; Supplementary Table S3). Concentrations of GA_{44} and GA_{19} were significantly lower in the *ga3ox2* mutant, consistent with increased GA20OX activity (Fig. 2A; Supplementary Table S3). Transcript levels of *GA20OX1* and *GA20OX2* were significantly higher in *ga3ox2* mutants compared with wild-type 'Cadenza', whereas several *GA2OX* genes were down-regulated, consistent with reduced feedback regulation in response to low bioactive GA concentrations (Supplementary Table S4).

In the glasshouse, *ga3ox2* plants were severely dwarfed (previously shown in Shani *et al.*, 2024) and had darker leaves and significantly more tillers than wild-type plants ($P<0.001$) (Fig. 2B, C). Reproductive development was severely delayed in the *ga3ox2* mutant, most prominently in the stages preceding terminal spikelet formation (Stage W3.5; Waddington *et al.*, 1983) (Supplementary Fig. S2). Upon emergence, *ga3ox2* spikes were compact, had significantly fewer spikelets than the

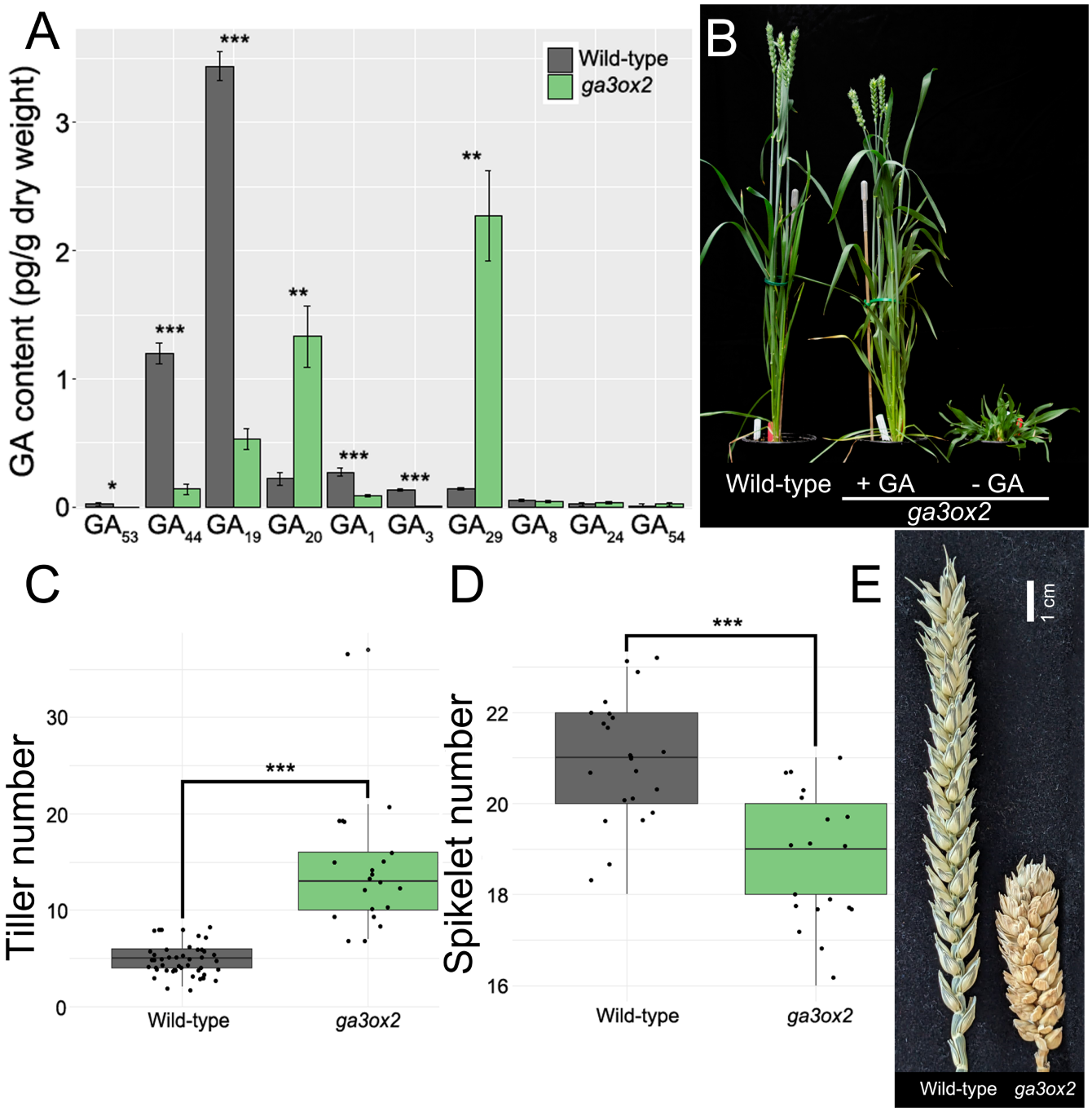

Fig. 2. Functional characterization of the *ga3ox2* mutant in wheat. (A) Quantification of gibberellin (GA) concentrations in wild-type and *ga3ox2* seedling tissues. (B) Phenotype of representative wild-type and *ga3ox2* plants when wild-type plants reached anthesis. The plant labelled '+ GA' was sprayed twice weekly with 10 μM GA_3. (C) Tiller number in wild-type and *ga3ox2* mutants (n=20). (D) Spikelet number in wild-type and *ga3ox2* mutants (n=20). (E) Representative spikes of wild-type and *ga3ox2* mutants taken post-anthesis. Bar=1 cm. Asterisks indicate significant differences between 'Cadenza' and *ga3ox2* genotypes (*P<0.05, **P<0.01, ***P<0.001; two-tailed Student's t-test).

wild type (P<0.001), and did not set seed (Fig. 2D, E). Twice-weekly sprays of bioactive GA_3 almost completely restored the height and fertility of *ga3ox2* mutants to those of the wild type, demonstrating that the observed phenotypes are caused by GA deficiency (Fig. 2B). Plants carrying loss-of-function mutations in two of three *GA3OX2* homoeologues were only between 1% and 9% shorter than the wild type, demonstrating that *GA3OX2* genes exhibit functional redundancy and that mutations in all three homoeologues are required to confer a severely dwarfed phenotype (Supplementary Fig. S3). Taken

together, these observations demonstrate that GA3OX2 activity is essential for normal vegetative and reproductive development in wheat.

Generation of *ga3ox3* and *ga1ox1* mutants

In the 'Cadenza' genome, *GA3OX3-A1* and *GA3OX3-B1* are predicted to encode full-length functional 2-ODD enzymes. However, *GA3OX3-D1* carries a 7 bp insertion in exon 2 that results in the introduction of a premature stop codon upstream of the conserved Fe^{2+} 2-ODD domain and likely encodes a non-functional protein (Supplementary Fig. S1A). Therefore, wheat plants carrying EMS-induced mutations introducing premature stop codons in *GA3OX3-A1* and *GA3OX3-B1*, respectively, were intercrossed and then backcrossed to develop a *ga3ox3* mutant (Table 1). A third EMS-mutated line carrying a point mutation in the 3′ splice acceptor site in intron 2 of *GA1OX1-B1* was backcrossed to develop a *ga1ox1* mutant (Table 1; Supplementary Fig. S1B). In the 'Cadenza' genome, *GA3OX3-B1* and *GA1OX1-B1* are just 3618 bp apart on chromosome 2B (Supplementary Fig. S4), precluding the recombination of these alleles into the same background, so *ga3ox3* and *ga1ox1* mutant lines were evaluated separately.

Sequential GA1OX1-B1 and GA3OX3 activity is required for GA_{54} and GA_{55} synthesis in wheat grains

Transcripts of *GA3OX3* and *GA1OX1* are detected almost exclusively in developing grain tissues (Pearce *et al.*, 2015), so we quantified GA concentrations in grains at 25 DPA, the stage at which grain filling reaches its maximum rate. Grains of wild-type plants accumulated extremely high concentrations of GA_{54} and GA_{55} and low concentrations of GA_{61} and GA_{60}, consistent with strong GA3OX3 and GA1OX1 activity in both the 13-OH and 13-H branches of the GA biosynthetic pathway (Fig. 3). By contrast, GA_{54} and GA_{55} concentrations were negligible in the *ga3ox3* mutant, and the GA3OX3 substrates GA_{61} and GA_{60} accumulated to high concentrations (Fig. 3). Notably, GA_{54} and GA_{55} concentrations were significantly reduced in the *ga3ox3-b1* mutant line ($P<0.001$) but not in the *ga3ox3-a1* mutant line ($P>0.05$) (Supplementary Table S5). These results demonstrate that GA3OX3 activity is required for the 3β-hydroxylation of GA_{61} to GA_{54} and of GA_{60} to GA_{55}, and that *GA3OX3-B1* contributes the majority of this activity.

The *ga1ox1* mutant also exhibited a significant reduction in GA_{54} and GA_{55} concentrations compared with the wild type, and neither GA_{60} nor GA_{61} was detected in this line, demonstrating that both GA3OX3 and GA1OX1 activity is required for GA_{54} and GA_{55} synthesis (Fig. 3). Since *GA1OX1* genes are found only in the B genome, we tested the capacity of different wheat species to synthesize GA_{54}. Using targeted analysis, we detected GA_{54} in the grain of hexaploid bread wheat (genomes AABBDD) and tetraploid durum wheat [*T. turgidum* ssp. *durum* (AABB)] but not in *T. urartu* (AA) or *A. tauschii* (DD) (Supplementary Fig. S5).

Changes in the concentrations of GA_{55} and GA_{60} in the *ga3ox3* and *ga1ox1* mutants mirrored those of GA_{54} and GA_{61}, but the 13-OH GAs were present at lower concentrations than their 13-H analogues, indicating that the 13-H GA pathway predominates in wheat grain (Fig. 3). We investigated the influence of the 13-hydroxyl group on GA 1-hydroxylase activity by incubating GA_9, GA_{20}, GA_4, and GA_1 with recombinant TaGA1OX1. GA_4 and GA_1 were not converted, further confirming the necessity for 1β-hydroxylation to precede 3β-hydroxylation in the formation of GA_{54} and GA_{55}. The enzyme converted GA_9 to GA_{61} and GA_{20} to GA_{60}; kinetic parameters are displayed in Supplementary Table S6. The k_{cat}/K_m values for GA_9 and GA_{20} were 8.7×10^{-3} μM^{-1} s^{-1} and 5.1×10^{-3} μM^{-1} s^{-1}, respectively, indicating a slight preference for GA_9 as the substrate. The dissociation constants (K_d values) for GA_9 and GA_{20} with TaGA1OX1 were determined using microscale thermophoresis as 1.2 μM and 4.8 μM, respectively (Supplementary Table S6).

Taken together, these results demonstrate that the sequential activity of GA1OX1-B1 and GA3OX3 is necessary and sufficient to catalyse $GA_9/GA_{20} \rightarrow GA_{61}/GA_{60} \rightarrow GA_{54}/GA_{55}$ reactions in wheat grain, and that most of this activity is performed by enzymes encoded by adjacent *GA1OX1-B1* and *GA3OX3-B1* genes on chromosome 2B.

GA3OX3 and GA1OX1 activity modulates bioactive GA concentrations during grain development

Bioactive GA_1 and GA_4 concentrations were significantly lower in the *ga3ox3* mutant than in the wild type ($P<0.001$), demonstrating that GA3OX3 catalyses the 3β-hydroxylation of GA_{20} to GA_1 and of GA_9 to GA_4 in wheat grain (Fig. 3; Supplementary Table S5). Concentrations of GA_{51} were significantly higher in the *ga3ox3* mutant ($P<0.001$), suggesting that in the absence of GA3OX3 activity, the substrate GA_9 is subject to higher rates of 2β-hydroxylation than in the wild type (Fig. 3). By contrast, bioactive GA_1 and GA_4 concentrations were extremely high in the *ga1ox1* mutant compared with wild-type segregants (Fig. 3). The *ga1ox1* mutant also accumulated significantly higher concentrations of precursor (e.g. GA_9) and inactivated (e.g. GA_{34}) forms of GA in both the 13-H and 13-OH pathways (Fig. 3).

GA3OX3 and GA1OX1 activity regulates grain development and stem elongation

To determine how differences in grain GA concentrations affect plant phenotype, we evaluated *ga1ox1* and *ga3ox3* mutants in field experiments in 2021 and 2023. Across both experiments, grains from the *ga1ox1* mutant were significantly wider, longer, and larger than those of the wild-type segregant, although the effects on TGW were inconsistent between

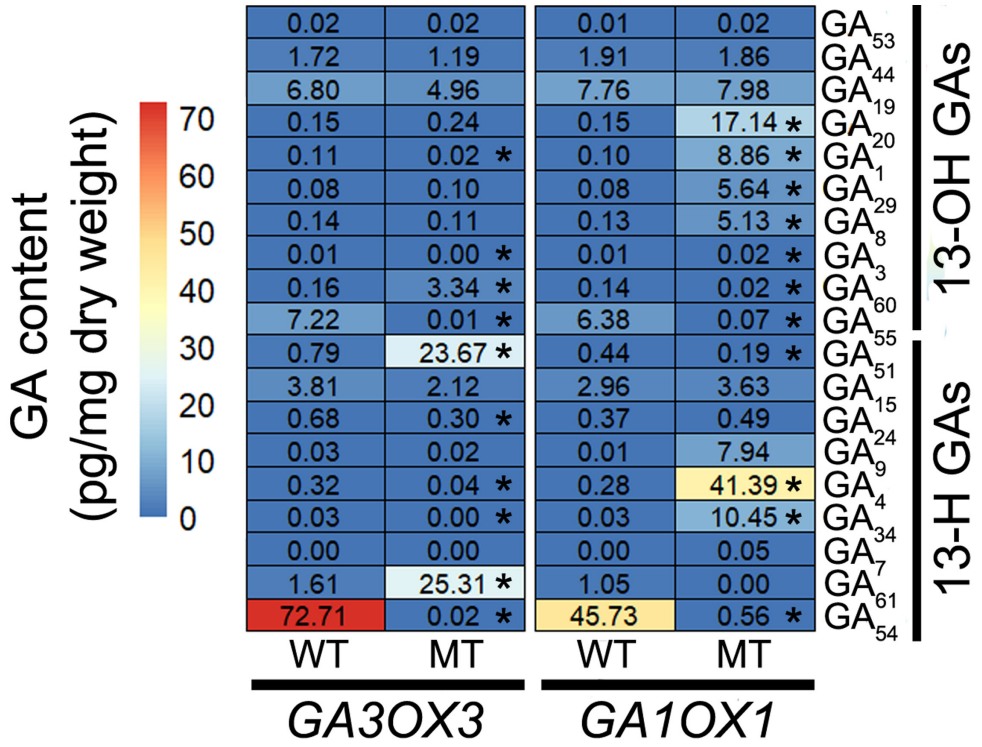

Fig. 3. Mean gibberellin (GA) concentrations in the grains of wild-type (WT) and *ga3ox3* and *ga1ox1* mutants (MT). Asterisks indicate significant differences between wild-type and mutant genotypes (*P<0.05; two-tailed Student's t-test).

different experiments, potentially due to environmental variation between years and the inherent variation in small-plot field experiments (Fig. 4A–D; Supplementary Table S7). By contrast, grain width and TGW were significantly lower in the *ga3ox3* mutant than in the wild-type segregant (Fig. 4A–D; Supplementary Table S7). Despite the differences in grain size, there were no significant differences between mutant and wild-type genotypes in yield (Supplementary Table S8). Nor were there any differences in spikelet number or grain number, suggesting that these genes do not influence inflorescence development (Supplementary Table S8).

Unexpectedly, the *ga3ox3* and *ga1ox1* mutations conferred differences in plant height. The *ga3ox3* mutants were 3.0 cm and 4.5 cm shorter (P=0.013) than their wild-type segregants, while the *ga1ox1* mutants were 10.7 cm (P<0.001) and 1.2 cm taller than their wild-type segregant lines in the 2021 and 2023 experiments, respectively (Fig. 4E; Supplementary Table S7). Changes in plant height were consistent when these lines were grown in glasshouse conditions (Supplementary Fig. S6).

To understand the basis of these height differences, we measured spike and individual internode lengths across the stem. In the *ga3ox3* mutant, the four lowest internodes were all significantly shorter than in the wild-type segregant (P≤0.018), whereas spike length was not affected (Fig. 4F; Supplementary Table S8). In the *ga1ox1* mutant, the spike was significantly longer than in the wild-type segregant (P=0.036), and the peduncle and P-1 internode were also longer, although these differences were not statistically significant. The lowest three internodes were all shorter in the *ga1ox1* mutant compared with the wild-type segregant (Fig. 4F; Supplementary Table S8). Taken together, these results show that the depletion of bioactive GA in the grains of *ga3ox3* mutants confers reduced height and TGW, while the accumulation of bioactive GA in *ga1ox1* mutants confers increased height and larger grains.

GA3OX2 genes are highly conserved in wheat genomes but *GA3OX3* and *GA1OX1* are genetically diverse

We next explored the genetic variation in wheat *GA3OX* genes. *GA3OX2* presents as a homoeologous triad in the genomes of all the modern and ancestral wheat species analysed, with no presence–absence variation (Supplementary Table S2). In the 'Cadenza' genome, homoeologous *GA3OX2* genes encode proteins that share >96% amino acid identity with one another (Supplementary Fig. S7). *GA3OX2* genes are also remarkably homogeneous within *T. aestivum* accessions. In the Watkins collection of 1051 wheat varieties and landraces, a single haplotype of *GA3OX2-A1* was shared by 96.3% of accessions (Supplementary Fig. S8) and across all three *GA3OX2* homoeologues, only five polymorphisms fall in protein-coding sequences (Supplementary Fig. S8).

By contrast, *GA3OX3* and *GA1OX1* are more genetically diverse among wheat accessions. Proteins encoded by the

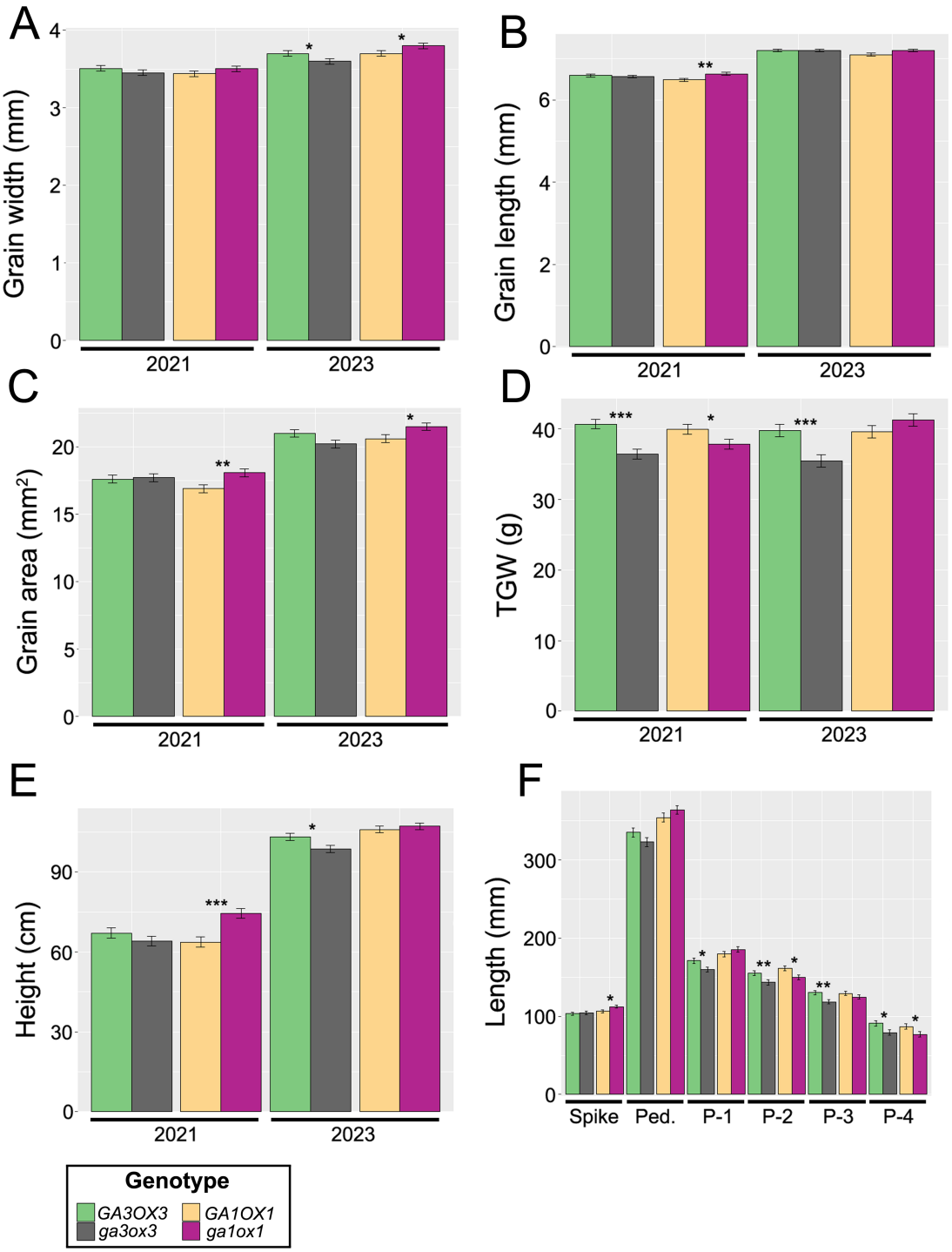

Fig. 4. Phenotype of *GA3OX3* and *GA1OX1* mutants in field experiments in 2021 and 2023. (A) Grain width. (B) Grain length. (C) Grain area. (D) Thousand-grain weight (TGW). (E) Plant height. (F) Length of individual stem components from the 2023 experiment. Plotted values represent predicted means ±SE. Asterisks indicate significant differences between the wild type and the corresponding mutant (*<*P*<0.05, **<*P*<0.01, ***<*P*<0.001; from nested contrasts extracted from the ANOVA). Ped., peduncle; P-1, P-2, P-3, P-4, first to fourth highest subsequent internodes. Supplementary Tables S7 and S8 include full data and statistical analysis.

GA3OX3-A1 and *GA3OX3-B1* homoeologues share only 83.7% identity at the amino acid level, and *GA1OX1-B1* is even less similar (Supplementary Fig. S7). *GA3OX3-D1* was either deleted or predicted to encode a non-functional protein in all screened hexaploid wheat accessions and *A. tauschii* (Supplementary Table S2). Both *GA3OX3-B1* and

GA1OX1-B1 genes were found in the B genomes of all common wheat varieties, durum wheat (*T. durum*), and wild emmer wheat (*T. dicoccoides*), as well as the S genomes of *A. speltoides*, *A. sharonensis*, and *A. longissimi*, and the G genome of *T. timopheevii* (Supplementary Table S2). This demonstrates that the duplication that originated *GA1OX1-B1* pre-dates the domestication of common wheat.

We focused on the genetic diversity at the *GA3OX3-B1-GA1OX1-B1* locus because of the dominant role of these genes in GA biosynthesis in the grain. In the Watkins collection, 58 haplotypes at this locus were shared by two or more accessions (Supplementary Table S9). The two most common haplotypes (H1, n=37 and H2, n=36) were polymorphic at 362 sites, including 53 variants within the *GA3OX3-B1* and *GA1OX1-B1* coding sequence (Supplementary Table S9). The GA3OX3-B1 proteins encoded by each haplotype share just 96.0% identity at the amino acid level, and the GA1OX1-B1 proteins are 95.8% identical.

In addition to variation in the protein-coding sequences, three non-coding regions were deleted in H2: a region approximately 562 bp downstream of *GA1OX1-B1*, a ~1842 bp intergenic region, and a region beginning 362 bp upstream of *GA3OX3-B1* (Fig. 5A). To study the frequency of these indels, we selected one polymorphic site for each of the three deleted regions and re-ran haplotype analysis in the Watkins landrace collection (Fig. 5A; Supplementary Table S10). There were five haplotypes shared by more than 10 accessions (Fig. 5B). Haplotypes were unevenly distributed across ancestral groups (χ^2=361.87, 28 df, P<0.001, n=1022). Across all accessions, H1, characterized by the deletion of all three regions, was the most common and was carried by 78.6% of modern wheat varieties (Fig. 5C; Supplementary Table S11). Among landraces, H1 was also the most common haplotype in all ancestral groups except groups 1 and 3, where H2, characterized by the presence of all sequences in these three regions, was the most common (Fig. 5C). H3 was carried by 31.5% of the accessions in ancestral group 6 (Fig. 5C). Haplotype frequencies also varied geographically (χ^2=360.77, 28 df, P<0.001, n=1017). In most regions, H1 was the most common haplotype, but H2 was carried by 40.2% of lines originating in Asia and H3 was carried by 44.4% of lines originating in Australia (Supplementary Fig. S9; Supplementary Table S11).

Among landraces, variation at the *GA3OX3-B1-GA1OX1-B1* locus was associated with differences in grain width, grain area, grain weight, and yield (Supplementary Table S12). Landraces carrying H1 exhibited, on average, significantly larger and heavier grains, as well as improved yield, than landraces carrying H2 or H3, but were not significantly different from those carrying haplotypes H4 or H5 (Fig. 5D, E; Supplementary Table S12). This finding suggests that this locus may have been subject to selection in modern wheat varieties.

Discussion

Orthologous *GA3OX2* genes play conserved roles in plant development

Genetic variation in GA biosynthesis genes has been an important source of reduced height and lodging resistance alleles in cereal crops (Hedden, 2003). These include *sd1*, a loss-of-function *OsGA20OX2* allele in rice (Sasaki *et al.*, 2002), and *Rht14*, caused by the misexpression of *TaGA2OX-A9* in wheat (Tian *et al.*, 2022). By contrast, allelic variation in *GA3OX* genes is less frequently deployed in breeding programmes, potentially because mutant alleles confer a reduction in height that is too extreme for use in crop production. The severely dwarfed phenotype of the wheat *ga3ox2* mutant is similar to that of the *d18-AD* and *d18-y* alleles in rice (which carry a deletion and a frameshift mutation in *OsGA3OX2*, respectively) and the *d1-6016* allele in maize (*Zea mays*) (which carries a deletion of *ZmGA3OX2*) (Itoh *et al.*, 2001; Sakamoto *et al.*, 2004; Teng *et al.*, 2013). These common phenotypes indicate that orthologous *GA3OX2* genes play functionally conserved roles in stem elongation in different cereal crops.

It is possible that mutations that reduce but do not abolish *GA3OX2* activity may have agronomic potential. For example, in rice, a 9 bp in-frame deletion in the *d18h* allele, an amino acid substitution in the *d18k* allele, and CRISPR-induced lesions in the *OsGA3OX2* promoter all confer a semi-dwarf phenotype (Itoh *et al.*, 2001; Sakamoto *et al.*, 2004; Zhou *et al.*, 2023). Similarly, in pea (*Pisum sativum*), an amino acid substitution in *LE,* which encodes a GA3OX enzyme, underlies the dwarf trait studied by Mendel (Lester *et al.*, 1997; Martin *et al.*, 1997). In maize, polymorphisms in the *ZmGA3OX2* promoter are associated with mild variation in plant height (Teng *et al.*, 2013). Mutations that introduce amino acid substitutions in wheat GA3OX2 proteins or combine loss-of-function alleles in one or two homoeologues may be one strategy to develop novel semi-dwarfing alleles for wheat production.

It is important to note that while rice plants carrying the most extreme *d18* alleles still set seed (Itoh *et al.*, 2001; Sakamoto *et al.*, 2004), the wheat *ga3ox2* mutant is infertile (Fig. 2E). This difference is likely due to the expression profile of paralogous *GA3OX* genes in each species. Whereas *OsGA3OX1* likely contributes to 3β-hydroxylase activity in the developing panicle (Sakamoto *et al.*, 2004; Kawai *et al.*, 2022), *TaGA3OX2* is the only wheat *GA3OX* gene expressed in the inflorescence and is therefore essential for fertility (Pearce *et al.*, 2015).

This essential role in both vegetative and reproductive development likely accounts for the extremely low levels of genetic diversity in the *GA3OX2* genes in wheat and suggests that they are highly constrained evolutionarily. Therefore, while the GA-deficient *ga3ox2* mutants may prove useful as a research tool to characterize GA responses, they are unlikely to be a rich source of variation for agronomically valuable alleles in wheat.

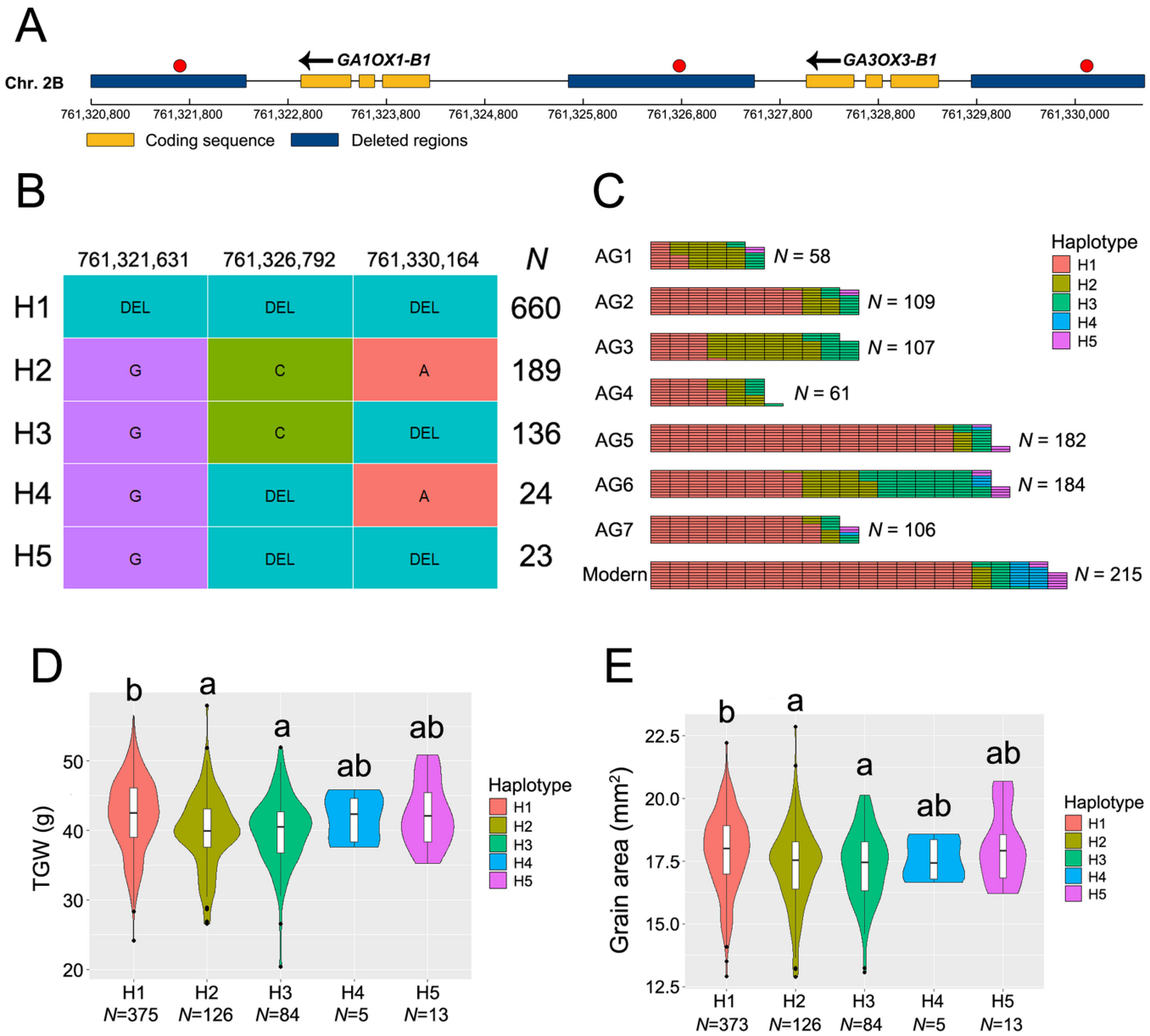

Fig. 5. Natural variation at the *GA3OX3-B1-GA1OX1-B1* locus. (A) The *GA3OX3-B1-GA1OX1-B1* locus in wheat. The transcriptional direction of each gene is indicated above the yellow boxes and the positions of the three putative deleted regions in some varieties are shown in blue. Red circles indicate the positions of three selected markers to distinguish the presence and absence of each deleted region. (B) Haplotype (H) frequency in the Watkins population based on the three markers (n=1032). (C) Haplotype frequency by ancestral group (AG) (n=1022). (D, E) Association between *GA3OX3-B1-GA1OX1-B1* haplotype and (D) thousand-grain weight (TGW) and (E) grain area in 603 accessions grown in the field in 2022. Different letters indicate significant differences between groups (P<0.05; Tukey's Honest Significant Difference post hoc test).

GA3OX3 exhibits 3β-hydroxylase activity during wheat grain development

Hormone profiling indicated that both *GA3OX3-A1* and *GA3OX3-B1* encode functional GA 3β-hydroxylases that contribute to bioactive GA_1 and GA_4 synthesis in the developing grain (Fig. 3; Supplementary Table S5). This is contrary to results from earlier *in vitro* studies, which detected no GA 3β-hydroxylase activity using the recombinant GA3OX3-A1 protein, potentially due to low *in vitro* expression in the heterologous system used to test this activity (Pearce *et al.*, 2015). Although both *GA3OX2* and *GA3OX3* exhibit GA 3β-hydroxylase activity, the phenotype of the *ga3ox3* mutant was much milder than that of *ga3ox2*, likely because of differences in gene expression patterns. *ga3ox3* mutants exhibit a mild reduction in plant height in both field and glasshouse conditions (Fig. 4; Supplementary Fig. S6). This finding is consistent with observations of barley plants carrying loss-of-function

mutations in the orthologue *HvGA3,18OX1*, which also have reduced bioactive GA_4 concentrations in grain tissues and slightly reduced height (Cheng *et al.*, 2023).

However, unlike the *ga3ox3* mutant in wheat, the barley *hvga3,18ox1* mutant showed no reduction in TGW (Cheng *et al.*, 2023). The difference in these observed phenotypes might arise from the functional divergence of these genes in barley and wheat. Whereas *HvGA3,18OX1* encodes a bifunctional GA 3β,18-dihydroxylase, catalysing the conversion of GA_9 to GA_{131}, GA3OX3 enzymes in wheat exhibit only 3β-hydroxylase activity, so that the mutant lines have different GA profiles (Pearce *et al.*, 2015). A tandem duplication on chromosome 2B originated *GA1OX1-B1*, which encodes an enzyme with altered function in GA biosynthesis that is specific to wheat.

Our genetic analyses demonstrate that GA3OX3 and GA1OX1-B1 activity is necessary and sufficient for $GA_{54/55}$ and $GA_{60/61}$ synthesis in wheat grains, with the 13-H pathway predominating in these tissues (Supplementary Table S5). Concentrations of GA_{54} and GA_{55} are significantly reduced in the *ga3ox3-b1* mutant but not in the *ga3ox3-a1* mutant, showing that GA3OX3-B1 is the more important enzyme catalysing these reactions (Supplementary Table S5). By contrast, GA_1 and GA_4 concentrations are significantly reduced in both *ga3ox3-a1* and *ga3ox3-b1* mutants, suggesting that both homoeologues contribute equally to catalysing the GA_9 to GA_4 and GA_{20} to GA_1 reactions (Supplementary Table S5). This difference could be due to protein sequence variation that allows GA3OX3-A1 to discriminate between the substrates GA_9/GA_{20} and GA_{60}/GA_{61}, whereas GA3OX3-B1 uses either substrate indiscriminately. Therefore, the majority of the grain-specific synthesis of GA_{54} and GA_{55} is catalysed by the sequential activity of GA3OX3-B1 and GA1OX1-B1 proteins encoded by linked genes on chromosome 2B that are inherited in the same haplotypic block.

This duplication is ancient and pre-dates the domestication of common wheat (Supplementary Table S2). The retention of both genes in all modern wheat varieties is consistent with the functional role of this locus during wheat development. The *ga1ox1* mutant, which lacks both GA_{54} and GA_{61}, sheds light on the physiological relevance of this pathway. The *ga1ox1* mutant accumulates extremely high concentrations of bioactive GA, and has slightly larger grains and an increase in the length of the spike and upper stem internodes relative to the wild type (Fig. 4). Based on these observations, it is tempting to speculate that the dual activity of GA3OX3 and GA1OX1 enzymes in grain tissues is a mechanism to modulate the concentrations of bioactive GA during grain development, potentially to moderate its effects on excessive stem elongation, which might confer improved performance in some environments.

The absence of *GA1OX1* transcripts in peduncle tissues in 'Cadenza' suggests the possibility that bioactive GA is transported from developing grains to stem tissues during the stem elongation phase. Although there are no documented examples of the transport of GAs from developing seeds, GA transport is an important mechanism regulating different stages of plant growth and development (Binenbaum *et al.*, 2018). It will be important to perform more detailed transcriptional and GA profiling to determine the basis for enhanced stem elongation in the *ga3ox3* and *ga1ox1* mutants.

Exploiting genetic variation at the *GA3OX3-B1-GA1OX1-B1* locus

Variation in the *GA3OX3-B1-GA1OX1-B1* locus is associated with differences in grain size, grain weight, and yield among common wheat landraces (Fig. 5D, E). Haplotype 1, which is associated with higher yields, is present at high frequencies in modern wheat germplasm, which might reflect a recent selection of this allele by breeders. However, it is also possible that these allele frequencies reflect the narrow base of selection in modern wheat germplasm. Ancestral groups 2 and 5, which contributed the most genetic diversity for modern wheat varieties (Cheng *et al.*, 2024), also exhibit a high frequency of this haplotype (Fig. 5C). Therefore, introgressing the alleles from haplotypes 4 and 5, which are rare among modern wheat accessions but are associated with high mean grain size and yield in landraces (Fig. 5; Supplementary Table S12), might be one approach to exploit novel variation at this locus.

The functional effects of the allelic variation on gene activity are less clear. The GA3OX3-B1 and GA1OX1-B1 proteins encoded by each allele have a low level of identity at the amino acid level and may exhibit different enzymatic activities. It is also possible that the structural rearrangements in the promoter regions of these genes confer differences in their spatial or temporal expression profiles. In a panel of 30 wheat varieties (Nirmal *et al.*, 2017), both H1 and H2 alleles of *GA3OX3-B1* and *GA1OX1-B1* were expressed at high levels in grain tissues at 14 DPA (Supplementary Fig. S10).

The regulatory variation that results in the expression of these genes in vegetative tissues might account for the differences in height seen in the *ga1ox1* and *ga3ox3* mutants, as well as the residual concentrations of bioactive GA_1 detected in the *ga3ox2* mutant line (Fig. 2A). It will also be interesting to study the effects of this variation on root development, as a low level of *GA1OX1-B1* transcripts was previously detected in growing roots (Ptošková *et al.*, 2022). Contrasting the expression profile of these alleles using biparental populations segregating for the major regulatory variants detected in this study provides an excellent system to test these hypotheses.

Supplementary data

The following supplementary data are available at *JXB* online.

Fig. S1. Effect of EMS-induced mutations in *GA3OX2*, *GA3OX3*, and *GA1OX1* genes in wheat.

Fig. S2. Inflorescence development in *ga3ox2* mutants.

Fig. S3. Height of *ga3ox2* mutants in glasshouse conditions.
Fig. S4. Physical location of *GA3OX3* and *GA1OX1-B1* genes on homoeologous group 2 chromosomes.
Fig. S5. Detection of GA_{54} in developing grain of different wheat species.
Fig. S6. Height of *ga3ox3* and *ga1ox1* mutants in glasshouse conditions.
Fig. S7. Amino acid identity of *GA3OX* genes in wheat.
Fig. S8. Haplotype analysis of *GA3OX2* genes in wheat accessions.
Fig. S9. Geographic distribution of *GA3OX3-B1-GA1OX1-B1* haplotypes.
Fig. S10. Grain expression levels of *GA3OX3-B1* and *GA1OX1-B1* in 30 wheat accessions.
Table S1. Genotyping markers used in this study.
Table S2. Presence/absence variation in *GA3OX2*, *GA3OX3*, and *GA1OX1-B1* in different wheat lines.
Table S3. GA concentrations in seedling tissues of *ga3ox2* mutant and 'Cadenza' lines.
Table S4. Transcript levels of GA biosynthesis genes in 'Cadenza' and *ga3ox2* mutant seedlings.
Table S5. GA concentrations in grain tissues of *ga1ox1* and *ga3ox3* mutants compared with their wild-type segregant lines.
Table S6. Kinetic parameters for TaGA1OX1 with substrates GA_9 and GA_{20}.
Table S7. Phenotypic analysis of grain traits and height in the 2021 and 2023 field experiments.
Table S8. Phenotypic analysis of inflorescence and grain traits in the 2023 field experiment.
Table S9. Haplotypes of *T. aestivum* at the *GA3OX3-B1-GA1OX1-B1* locus (all markers).
Table S10. Haplotypes of *T. aestivum* at the *GA3OX3-B1-GA1OX1-B1* locus (three markers).
Table S11. *GA3OX3-B1-GA1OX1-B1* haplotype frequency in ancestral groups and region of origin.
Table S12. Haplotype–trait associations for selected phenotypes.

Acknowledgements

We are grateful to Andrew Mead for assistance and advice on statistical analysis and to the field teams and glasshouse staff for the management of the field trials and controlled-environment experiments. We are further grateful for the technical assistance of Renata Plotzova during the sample preparation for UHPLC-MS/MS analysis of GA.

Author contributions

ALP, SGT, PH, SP: conceptualization; ALP, AKH, SJC, PJ, DT, AR, SP: formal analysis; PH, ALP, SGT, MJH, SP: funding acquisition; ALP, AKH, RAR, PJ, PS, DT, DS: investigation; ALP, PH, SP: project administration; MJH, AR, DS: resources; ALP, PH, SGT, SP, MJH, AR: supervision; SP, ALP, PH: visualization; SP: writing—original draft and preparation; ALP, SJC, PJ, DT, PH, SP: writing—review and editing.

Conflict of interest

The authors declare no conflict of interest.

Funding

This project was funded by the Biotechnology and Biological Sciences Research Council (BBSRC) through the Delivering Sustainable Wheat (BB/X011003/1) and Designing Future Wheat (BB/P016855/1) programmes, and by the European Regional Development Fund Project No. CZ.02.01.01/00/22_008/0004581 (TowArds Next GENeration Crops; https://www.tangenc.cz).

Data availability

The data generated in this study and statistical analyses are provided in the manuscript and supplementary tables. All plant materials used in this study are available upon request from the corresponding author.

References

Appleford NEJ, Evans DJ, Lenton JR, Gaskin P, Croker SJ, Devos KM, Phillips AL, Hedden P. 2006. Function and transcript analysis of gibberellin-biosynthetic enzymes in wheat. Planta **223**, 568–582.

Avni R, Lux T, Minz-Dub A, *et al*. 2022. Genome sequences of three *Aegilops* species of the section Sitopsis reveal phylogenetic relationships and provide resources for wheat improvement. The Plant Journal **110**, 179–192.

Avni R, Nave M, Barad O, *et al*. 2017. Wild emmer genome architecture and diversity elucidate wheat evolution and domestication. Science **357**, 93–97.

Binenbaum J, Weinstain R, Shani E. 2018. Gibberellin localization and transport in plants. Trends in Plant Science **23**, 410–421.

Bolger AM, Lohse M, Usadel B. 2014. Trimmomatic: a flexible trimmer for Illumina sequence data. Bioinformatics **30**, 2114–2120.

Castro-Camba R, Sánchez C, Vidal N, Vielba JM. 2022. Plant development and crop yield: the role of gibberellins. Plants **11**, 2650.

Chen Y, Song W, Xie X, Wang Z, Guan P, Peng H, Jiao Y, Ni Z, Sun Q, Guo W. 2020. A collinearity-incorporating homology inference strategy for connecting emerging assemblies in the Triticeae tribe as a pilot practice in the plant pangenomic era. Molecular Plant **13**, 1694–1708.

Cheng J, Hill C, Han Y, He T, Ye X, Shabala S, Guo G, Zhou M, Wang K, Li C. 2023. New semi-dwarfing alleles with increased coleoptile length by gene editing of *gibberellin 3-oxidase 1* using CRISPR-Cas9 in barley (*Hordeum vulgare* L.). Plant Biotechnology Journal **21**, 806–818.

Cheng S, Feng C, Wingen LU, *et al*. 2024. Harnessing landrace diversity empowers wheat breeding. Nature **632**, 823–831.

de Lucas M, Davière JM, Rodríguez-Falcón M, Pontin M, Iglesias-Pedraz JM, Lorrain S, Fankhauser C, Blázquez MA, Titarenko E, Prat S. 2008. A molecular framework for light and gibberellin control of cell elongation. Nature **451**, 480–484.

Gaskin P, Kirkwood PS, Lenton JR, MacMillan J, Radley ME. 1980. Identification of gibberellins in developing wheat grain. Agricultural and Biological Chemistry **44**, 1589–1593.

Grewal S, Yang CY, Scholefield D, *et al*. 2024. Chromosome-scale genome assembly of bread wheat's wild relative *Triticum timopheevii*. Scientific Data **11**, 420.

Hedden P. 2003. The genes of the green revolution. Trends in Genetics **19**, 5–9.

Hsieh KT, Wu CC, Lee SJ, *et al*. 2023. Rice *GA3ox1* modulates pollen starch granule accumulation and pollen wall development. PLoS One **18**, e0292400.

Itoh H, Ueguchi-Tanaka M, Sentoku N, Kitano H, Matsuoka M, Kobayashi M. 2001. Cloning and functional analysis of two gibberellin 3β-hydroxylase genes that are differently expressed during the growth of rice. Proceedings of the National Academy of Sciences, USA **98**, 8909–8914.

Kaneko M, Itoh H, Inukai Y, Sakamoto T, Ueguchi-Tanaka M, Ashikari M, Matsuoka M. 2003. Where do gibberellin biosynthesis and gibberellin signaling occur in rice plants? The Plant Journal **35**, 104–115.

Kawai K, Takehara S, Kashio T, *et al*. 2022. Evolutionary alterations in gene expression and enzymatic activities of gibberellin 3-oxidase 1 in *Oryza*. Communications Biology **5**, 67.

Kawai Y, Ono E, Mizutani M. 2014. Evolution and diversity of the 2-oxoglutarate-dependent dioxygenase superfamily in plants. The Plant Journal **78**, 328–343.

Kirkwood PS, MacMillan J. 1982. Gibberellins A_{60}, A_{61}, and A_{62}: partial syntheses and natural occurrence. Journal of the Chemical Society, Perkin Transactions 1 **1982**, 689–697.

Krasileva KV, Vasquez-Gross HA, Howell T, *et al*. 2017. Uncovering hidden variation in polyploid wheat. Proceedings of the National Academy of Sciences, USA **114**, E913–E921.

Lester DR, Ross JJ, Davies PJ, Reid JB. 1997. Mendel's stem length gene (*Le*) encodes a gibberellin 3β-hydroxylase. The Plant Cell **9**, 1435–1443.

Ling HQ, Ma B, Shi X, *et al*. 2018. Genome sequence of the progenitor of wheat A subgenome *Triticum urartu*. Nature **557**, 424–428.

Love MI, Huber W, Anders S. 2014. Moderated estimation of fold change and dispersion for RNA-seq data with DESeq2. Genome Biology **15**, 550.

Luo MC, Gu YQ, Puiu D, *et al*. 2017. Genome sequence of the progenitor of the wheat D genome *Aegilops tauschii*. Nature **551**, 498–502.

Maccaferri M, Harris NS, Twardziok SO, *et al*. 2019. Durum wheat genome highlights past domestication signatures and future improvement targets. Nature Genetics **51**, 885–895.

MacMillan J, Ward DA, Phillips AL, Sánchez-Beltrán MJ, Gaskin P, Lange T, Hedden P. 1997. Gibberellin biosynthesis from gibberellin A_{12}-aldehyde in endosperm and embryos of *Marah macrocarpus*. Plant Physiology **113**, 1369–1377.

Martin DN, Proebsting WM, Hedden P. 1997. Mendel's dwarfing gene: cDNAs from the *Le* alleles and function of the expressed proteins. Proceedings of the National Academy of Sciences, USA **94**, 8907–8911.

Mitchum MG, Yamaguchi S, Hanada A, Kuwahara A, Yoshioka Y, Kato T, Tabata S, Kamiya Y, Sun TP. 2006. Distinct and overlapping roles of two gibberellin 3-oxidases in Arabidopsis development. The Plant Journal **45**, 804–818.

Nirmal RC, Furtado A, Rangan P, Henry RJ. 2017. Fasciclin-like arabinogalactan protein gene expression is associated with yield of flour in the milling of wheat. Scientific Reports **7**, 12539.

Pearce S, Huttly AK, Prosser IM, *et al*. 2015. Heterologous expression and transcript analysis of gibberellin biosynthetic genes of grasses reveals novel functionality in the *GA3ox* family. BMC Plant Biology **15**, 130.

Ptošková K, Szecówka M, Jaworek P, Tarkowská D, Petřík I, Pavlović I, Novák O, Thomas SG, Phillips AL, Hedden P. 2022. Changes in the concentrations and transcripts for gibberellins and other hormones in a growing leaf and roots of wheat seedlings in response to water restriction. BMC Plant Biology **22**, 284.

Sakamoto T, Miura K, Itoh H, *et al*. 2004. An overview of gibberellin metabolism enzyme genes and their related mutants in rice. Plant Physiology **134**, 1642–1653.

Sasaki A, Ashikari M, Ueguchi-Tanaka M, *et al*. 2002. A mutant gibberellin-synthesis gene in rice. Nature **416**, 701.

Schomburg FM, Bizzell CM, Lee DJ, Zeevaart JA, Amasino RM. 2003. Overexpression of a novel class of gibberellin 2-oxidases decreases gibberellin levels and creates dwarf plants. The Plant Cell **15**, 151–163.

Shani E, Hedden P, Sun T-P. 2024. Highlights in gibberellin research: a tale of the dwarf and the slender. Plant Physiology **195**, 111–134.

Shimada A, Ueguchi-Tanaka M, Nakatsu T, Nakajima M, Naoe Y, Ohmiya H, Kato H, Matsuoka M. 2008. Structural basis for gibberellin recognition by its receptor GID1. Nature **456**, 520–523.

Sponsel VM. 2016. Signal achievements in gibberellin research: the second half-century. Annual Plant Reviews **49**, 1–36.

Teng F, Zhai L, Liu R, Bai W, Wang L, Huo D, Tao Y, Zheng Y, Zhang Z. 2013. *ZmGA3ox2*, a candidate gene for a major QTL, *qPH3.1*, for plant height in maize. The Plant Journal **73**, 405–416.

Thomas SG, Phillips AL, Hedden P. 1999. Molecular cloning and functional expression of gibberellin 2-oxidases, multifunctional enzymes involved in gibberellin deactivation. Proceedings of the National Academy of Sciences, USA **96**, 4698–4703.

Tian X, Xia X, Xu D, *et al*. 2022. *Rht24b*, an ancient variation of *TaGA2ox-A9*, reduces plant height without yield penalty in wheat. New Phytologist **233**, 738–750.

Ueguchi-Tanaka M, Ashikari M, Nakajima M, *et al*. 2005. *GIBBERELLIN INSENSITIVE DWARF1* encodes a soluble receptor for gibberellin. Nature **437**, 693–698.

Urbanová T, Tarkowská D, Novák O, Hedden P, Strnad M. 2013. Analysis of gibberellins as free acids by ultra performance liquid chromatography–tandem mass spectrometry. Talanta **112**, 85–94.

Waddington SR, Cartwright PM, Wall PC. 1983. A quantitative scale of spike initial and pistil development in barley and wheat. Annals of Botany **51**, 119–130.

Walkowiak S, Gao L, Monat C, *et al*. 2020. Multiple wheat genomes reveal global variation in modern breeding. Nature **588**, 277–283.

Wang T, Li J, Jiang Y, *et al*. 2023. Wheat gibberellin oxidase genes and their functions in regulating tillering. PeerJ **11**, e15924.

Yu G, Matny O, Champouret N, *et al*. 2022. *Aegilops sharonensis* genome-assisted identification of stem rust resistance gene *Sr62*. Nature Communications **13**, 1607.

Zentella R, Zhang ZL, Park M, *et al*. 2007. Global analysis of DELLA direct targets in early gibberellin signaling in *Arabidopsis*. The Plant Cell **19**, 3037–3057.

Zhang R, Jia G, Diao X. 2023. geneHapR: an R package for gene haplotypic statistics and visualization. BMC Bioinformatics **24**, 199.

Zhou J, Liu G, Zhao Y, *et al*. 2023. An efficient CRISPR-Cas12a promoter editing system for crop improvement. Nature Plants **9**, 588–604.

Zhu T, Wang L, Rimbert H, *et al*. 2021. Optical maps refine the bread wheat *Triticum aestivum* cv. Chinese Spring genome assembly. The Plant Journal **107**, 303–314.